CHEMISTRY OF MATERIALS

Article

pubs.acs.org/cm

A Facile Mechanism for Recharging Li_2O_2 in Li–O_2 Batteries

ShinYoung Kang, Yifei Mo, Shyue Ping Ong, and Gerbrand Ceder*

Department of Materials Science and Engineering, Massachusetts Institute of Technology, Cambridge, Massachusetts 02139, United States

Supporting Information

ABSTRACT: Li–air is a novel battery technology with the potential to offer very high specific energy, but which currently suffers from a large charging overpotential and low power density. In this work, we use ab initio calculations to demonstrate that a facile mechanism for recharging Li_2O_2 exists. Rather than the direct decomposition pathway of Li_2O_2 into Li and O_2 suggested by equilibrium thermodynamics, we find an alternative reaction pathway based on topotactic delithiation of Li_2O_2 to form off-stoichiometric $Li_{2-x}O_2$ compounds akin to the charging mechanism in typical Li-ion intercalation electrodes. The low formation energy of bulk $Li_{2-x}O_2$ phases confirms that this topotactic delithiation mechanism is rendered accessible at relatively small overpotentials of ~0.3–0.4 V and is likely to be kinetically favored over Li_2O_2 decomposition. Our findings indicate that at the Li_2O_2 particle level there are no obstacles to increase the current density, and point to an exciting opportunity to create fast charging Li–air systems.

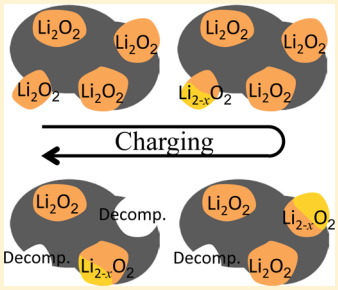

KEYWORDS: *Li–air batteries, charging mechanism, oxygen evolution reaction, lithium superoxide (LiO_2)*

1. INTRODUCTION

Li–air batteries, in which Li^+ ions react with oxygen, are an enticing novel rechargeable battery technology[1−4] offering the potential for high theoretical specific energy due to the low weight and high reaction energy of lithium metal. However, the technology is still in its infancy, and the scientific and technical challenges that remain to be overcome are described in several good reviews.[5−10] It has been well established that the overall reaction in a Li–O_2 cell is the oxidation of lithium to Li_2O_2 upon discharge and its subsequent reduction upon charge:[4−9,11−13]

$$2Li^+ + O_2 + 2e^- \underset{\text{charge}}{\overset{\text{discharge}}{\rightleftharpoons}} Li_2O_2 \quad (1)$$

However, very little is known about the detailed microscopic mechanisms by which these reactions proceed. Such understanding is needed to optimize the rate and cycle life, and decrease the large difference between the charge and discharge voltage that is currently needed to operate the cell. In particular, the large voltage hysteresis leads to large energy losses and would exclude Li–air as a viable technology for large batteries.[1−10,14]

While early work was often plagued by reactivity of the discharge products with the electrolyte solvent,[15−19] recent experiments performed in appropriately stable electrolytes have demonstrated the overall reaction as the formation of Li_2O_2 with little byproducts in discharge.[2,3,11,17−19] In discharge, characterization by in situ surface enhanced Raman spectroscopy (SERS) has shown that reduction of dissolved O_2 to O_2^- reacts with Li^+ to make LiO_2 ("lithium superoxide") that is not stable in the cell and disproportionates to Li_2O_2 and O_2.[20−22] The discharge curve is usually characterized by a relatively flat potential, which suggests a multiphase reaction process.[1−4,11,23,24]

Less is understood about the process by which the cell recharges, only that it requires a substantial overpotential. Direct evidence provided by differential electrochemical mass spectrometry (DEMS) and a variety of characterization techniques shows that the charging reaction involves the decomposition of Li_2O_2 to Li and O_2.[2,3,12,17,19,25,26] However, in contrast to the relatively flat potential in discharge, oxidization phenomena between 3.2 and more than 4 V have been seen in the charging process.[1−3,7−9,11−13,23,24,27,28]

More recent experiments have shown that O_2 evolution begins at relatively low charging voltage (as low as 3.1 V).[2,17,25,26] A clear plateau is observed at a voltage of 3.2–3.3 V in the charging curve.[2,3,26,27,29,30] A significant fraction of capacity (~30–50% of total discharged capacity) can be charged at this low-voltage plateau,[2,3,26,27,29,30] which is significantly lower than the previously reported charging voltage of 3.6 to more than 4 V. In addition, improved rate capability is reported in these studies with low charging overpotential. For example, refs 2, 3, and 29 have shown a ~10-fold improvement in the charging rate, and ref 17 has shown that the current associated with the peak at 3.2 V is 50–100% higher as compared to current peaks at higher voltages.

This recent progress has provided optimism that one of the key issues of Li–air batteries, its high charging overpotential, can be solved. A few charging mechanisms have been proposed to explain the low charging overpotential and improved kinetics. For instance, Hummelshøj et al.[31] suggested the

Received: May 28, 2013
Revised: July 29, 2013
Published: July 31, 2013

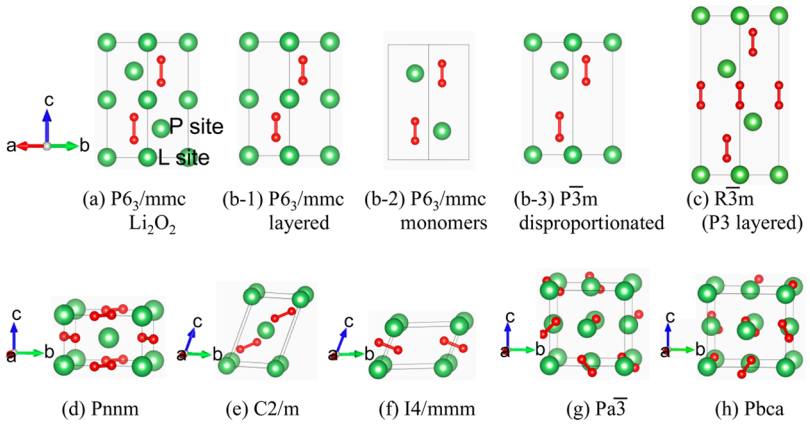

Figure 1. The structure for Li_2O_2 (a) and candidate structures for LiO_2 (b–h). Green spheres are lithium ions, and red spheres are oxygen ions. Oxygen bonds are marked as red bars. (a) Two distinct Li sites exist in the Li_2O_2 structure with $P6_3/mmc$ space group: a site that forms a Li-only layer (henceforth known as the "L" site), and a site in the plane that contains the peroxide bond centers (henceforth labeled as the "P" site). From (b) to (h), nine candidate LiO_2 structures are displayed. (b) The structures derived from Li_2O_2 by extracting two lithium ions from a Li_2O_2 unit cell; these structures are labeled by their symmetry; (c) layered P3 structure by removing Na and replacing Co with Li from P3 $NaCoO_2$; (d) marcasite structure; (e) $C2/m$ structure where Li and O_2^- ions layers are alternately stacked; (f) $I4/mmm$ structure where LiO_2 dimers are arranged in a bipyramid structure; (g) pyrite structure; and (h) a structure in *Pbca* space group, which has an arrangement of atoms similar to that in the pyrite structure, but in an orthorhombic lattice.

decomposition of Li_2O_2 particles at kink and step sites on surfaces to account for the low overpotential at the initial stage of charging. However, the density of kink and step sites is expected to be small on Li_2O_2 particles, which are as large as hundreds of nanometers in diameter.[12,32] More importantly, even if Li_2O_2 is preferentially removed at kink and step sites, this process will end as soon as the terrace that forms the kinks and steps is consumed in the charge.[3,6,11,17,26,33] On the other hand, a charging mechanism that involves the formation of LiO_2 as an intermediate has been proposed by Lu and Shao-Horn.[34] Recent studies by Yang et al.[30] have observed the existence of LiO_2-like species in the discharged product. These LiO_2-like species were attributed to the superoxide-like oxygen rich surfaces of Li_2O_2 and/or the small clusters of Li_2O_2. The superoxides were found to be the origin of the initial ~40% of charging capacity at a voltage plateau ~3.2–3.5 V, and the superoxides disappeared as soon as the sample is charged back to higher than 3.7 V. However, the decomposition path from Li_2O_2 through LiO_2 has not been clarified, nor how it can serve as a fast rate pathway at low overpotential. Thus, a key puzzle remains regarding what controls the overpotential and the kinetics in reduction.

While we confirm in this Article, using highly accurate ab initio computations, that eq 1 is indeed the equilibrium path, we also demonstrate that a more facile path for Li_2O_2 charging exists that requires only about 370 mV of overpotential, in good agreement with experiments. At this relatively small overpotential, the discharge product Li_2O_2 is delithiated topotactically to form off-stoichiometric $Li_{2-x}O_2$ compounds. We find that the formation of these off-stoichiometric states is energetically favorable and is likely to be kinetically easy. The previously predicted good electronic and ionic conductivity[35−41] in these off-stoichiometric states would further enhance delithiation until these products eventually break up into Li^+ and O_2 or O_2^- species, with possible dissolution in the electrolyte.[6,14,20,42] Because our findings show that the topotactic delithiation proceeds at constant or decreasing overpotential, and the rate capability of the peroxide increases as Li is removed, we further predict that the oxidation reaction will proceed locally in the electrode, with particles completely reacting once they have started to delithiate, leading to much larger current concentrations than would be expected from the average electrode current. This localization of current is a key factor in the rate capability of Li–O_2 batteries.

We provide a new perspective that at least in some part of its charge cycle, Li_2O_2 may be similar to more typical Li-transition metal intercalation cathodes, with O_2^{2-} being the redox active center that compensates for the removal of Li^+ ions.

2. COMPUTATIONAL METHODS

The total energies of compounds were calculated using the Vienna Ab-initio Simulation Package (VASP)[43] with the projector augmented-wave (PAW) method[44] and the Heyd–Scuseria–Ernzerhof (HSE) screened hybrid functional.[45,46] We used a screened exchange mixing parameter α of 0.207, the value proposed by the authors of the HSE06 functional.[47] The plane wave energy cutoff was set at 500 eV, and a k-point mesh was sampled with <0.05 Å^{-1} k-points spacing. All structures were relaxed until the total energies were converged to within 10^{-5} eV/atom.

In this study, we focus on $Li_{2-x}O_2$ ($0 < x < 1$) intermediates during charge as well as Li_2O, Li_2O_2, and LiO_2 stoichiometry compounds. The free energy of formation of a Li_aO_b compound is computed with respect to elemental chemical potentials as follows:

$$\Delta G_{f,Li_aO_b} = E_{Li_aO_b} - TS_{Li_aO_b} - a(E_{Li} - TS_{Li}) - \frac{b}{2}(E_{O_2} - TS_{O_2}) \quad (2)$$

where $E_{Li_aO_b}$, E_{Li}, and E_{O_2} are the total energies of the Li_aO_b compound, bulk metallic lithium, and an oxygen molecule as computed in HSE, T is temperature (298.15 K in this work), and $S_{Li_aO_b}$, S_{Li}, and S_{O_2} are the entropies of the Li_aO_b compound, bulk metallic lithium, and oxygen gas, respectively. The entropies of Li_2O, Li_2O_2, Li metal, and O_2 gas were obtained from the experimental values under standard conditions (298.15 K, 1 atm),[48] and are 0.39, 0.59, 0.30, and 2.13 meV/K per formula unit of Li_2O, Li_2O_2, Li, and O_2, respectively. Because there is no measured entropy for bulk LiO_2 or for the intermediate states $Li_{2-x}O_2$ ($0 < x < 1$), the entropy for LiO_2 was estimated from that of other alkali superoxides, and the entropies of intermediate states are linearly interpolated from the entropies of Li_2O_2 and LiO_2 (see the Supporting Information). The equilibrium voltage between inter-

dx.doi.org/10.1021/cm401720n | *Chem. Mater.* 2013, 25, 3328–3336

mediate compounds during charging, $Li_{2-x_1}O_2$ and $Li_{2-x_2}O_2$, is given by the following expression:[49]

$$U = -\frac{\Delta G_{f,Li_{2-x_1}O_2} - \Delta G_{f,Li_{2-x_2}O_2}}{(x_2 - x_1)F} \quad (3)$$

where F is the Faraday constant.

It is well-known that DFT, including DFT with the HSE functional,[50,51] underestimates the magnitude of formation energy of the metal oxides relative to experiments. This deficiency of DFT introduces errors in the formation energies of oxides, peroxides, and superoxides.[35,39] A measured formation energy of LiO_2 is not available from experiments to the best of our knowledge. Therefore, to correctly characterize the voltage of LiO_2 and the overpotential to form LiO_2, it is essential for our calculations to reproduce the correct voltages for oxides, peroxides, and superoxides at the same time. We adapted the fitting scheme introduced by Wang et al.[51] to correct for the errors in the formation energies of oxides, peroxides, and superoxides by fitting the calculated formation energies of a group of oxides, peroxides, and superoxides to their known experimental formation enthalpies (details provided in the Supporting Information). These correction terms thus obtained are 1.05 eV/O_2, 0.76 eV/O_2^{2-}, and 0.33 eV/O_2^- for oxides, peroxides, and superoxides, respectively, in HSE. With these new corrections and experimentally reported entropies, our calculations predict the voltages of Li_2O and Li_2O_2 to be 2.93 and 2.97 V, respectively, which are in excellent agreement with experimental voltages of 2.91 and 2.96 V for Li_2O and Li_2O_2, respectively.[48]

3. RESULTS

3.1. The Structure of Lithium Superoxide. The structure of lithium peroxide (Figure 1a) consists of close-packed layers of lithium ions stacked in an ABAC arrangement along the *c*-axis[52,53] and oxygen peroxide dimers aligned along the *c*-axis straddling one of the Li layers. There are two symmetrically distinct Li sites in Li_2O_2, which we have labeled P (Li site in the peroxide layer), L (Li site in the Li-only layer) in Figure 1a. This notation will be used throughout this Article. It has been previously established that in the Li_2O_2 structure, the P sites are higher in energy and therefore tend to be the favorable sites to form Li vacancies.[36,37,54]

While it is usually assumed that Li_2O_2 is stoichiometric, topotactic removal of Li with oxidation of O_2^{2-} to O_2^- is conceivable, as both oxidation states of O_2 exist. As this oxidation removes an antibonding electron, it results in a decrease in bond length of O_2, not unlike the size change of a transition metal ion in a Li-ion intercalation cathode when it is oxidized. We also observe that the structure of Li_2O_2 is similar to that of P2 $NaCoO_2$.[55] The Li_2O_2 structure can be obtained by substituting Na and Co cations in P2 $NaCoO_2$ for Li and decreasing the O−O bond distance to form peroxide bonds. P2 $NaCoO_2$ is a well-known intercalation electrode material in Na-ion batteries, indicating that Li_2O_2 could undergo topotactic delithiation as well. More specifically, oxidation of 2 O^{2-} to O_2^{2-} has recently been demonstrated computationally in Li_2MnO_3, lending further credence to the idea that topotactic Li removal with peroxide ion formation is possible in host structures.[56]

We proceed by first investigating the relative stability of various LiO_2 structures, and then proceed to determine the overpotential needed to form intermediates between LiO_2 and Li_2O_2. Nine possible structure types were evaluated as possible ground state for LiO_2:

(1) Three symmetrically distinct structures are obtained by extracting two Li atoms from a single Li_2O_2 unit cell (from Figure 1b-1 to b-3). The Li_2O_2 derivatives in Figure 1b are labeled by the symmetry of the relaxed structure and a descriptor of the main structure feature. For example, the structure labeled $P6_3/mmc$-layered in Figure 1b-1 has alternating Li and O_2 layers stacked along the *c*-axis. The $P6_3/mmc$-monomer structure in Figure 1b-2 comprises LiO_2 monomers. The $P\bar{3}m$-disproportionated structure in Figure 1b-3 is named after the fact that its relaxed final structure is a "disproportionated state", which resembles $1/2Li_2O_2 + 1/2O_2$ (see later for details).

(2) A $R\bar{3}m$ (P3 layered) structure is obtained by removing Na and replacing Co with Li from the layered P3 $NaCoO_2$ structure (Figure 1c).[55] Given the structural similarity between Li_2O_2 and P2 $NaCoO_2$, we investigated this analogue of the P3 structure as a candidate structure for ground state LiO_2.

(3) Additional structures from Figure 1d to h are obtained by substituting metal ions with Li in known superoxides and peroxides with AO_2 stoichiometry, such as NaO_2, KO_2, RbO_2, and CsO_2 as known superoxides, and BaO_2, CaO_2, CdO_2, HgO_2, MgO_2, SrO_2, and ZnO_2 as known AO_2 stoichiometry peroxides.

The computed HSE formation free energies for the candidate structures of LiO_2 are plotted in Figure 2 using eq 2. We find

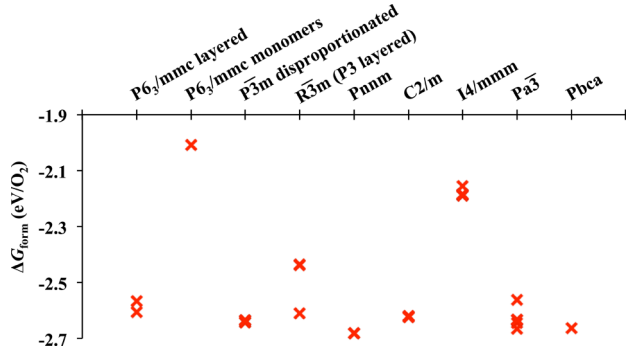

Figure 2. The calculated formation free energy (in eV/O_2) of the different structures considered for LiO_2. Multiple data points indicate the energies computed from different initial structures, such as NaO_2, CsO_2, MgO_2, etc., or from different magnetic states. The lowest energy structure is *Pnnm* (−2.68 eV/O_2).

that the marcasite structure in the *Pnnm* space group (Figure 1d) is the calculated ground-state structure for LiO_2, with a formation free energy of −2.68 eV/O_2. The ground-state structure is in agreement with an experimental diffraction study of LiO_2 at 4.2 K[57] and with previous computational studies on a small number of possible structures.[58,59] The lattice parameters of the *Pnnm* LiO_2 structure observed in experiments and computation are summarized in Table S1.

Furthermore, we find that lithium superoxide is not thermodynamically stable when the oxygen energy is set to represent oxygen gas at 1 atm and 298.15 K, as the lowest free energy at that composition is a combination of $1/2Li_2O_2 + 1/2O_2$. This result indicates that eq 1 is indeed the thermodynamically favored reaction at this condition,[58,59] and is consistent with the fact that LiO_2 has been observed to disproportionate into Li_2O_2 and O_2 during discharge.[2,21] Nevertheless, it is worth pointing out that this result will depend on the applied oxygen chemical potential. At high enough oxygen chemical potentials, for example, high oxygen partial pressure and/or low temperature, LiO_2 can become thermodynamically stable.

dx.doi.org/10.1021/cm401720n | Chem. Mater. 2013, 25, 3328−3336

The three LiO_2 structures derived from $P6_3/mmc$ Li_2O_2 are of interest in this study as they could be easily created by topotactic delithiation of Li_2O_2 during charging. Among these structures, we chose to neglect the $P\bar{3}m$-disproportionated structure, because it is a "disproportionated state", which resembles $1/2Li_2O_2 + 1/2O_2$. The disproportionation is confirmed by the fact that the lengths of two O_2 bonds in the unit cell are split into 1.21 and 1.51 Å, which are the typical bond lengths for O_2 and O_2^{2-}, respectively. When neglecting this structure, the $P6_3/mmc$-layered structure has the lowest energy among those derived from topotactically delithiating Li_2O_2. The formation free energy of this structure, −2.61 eV/O_2, indicates that topotactic removal of Li from Li_2O_2 is not much higher in energy than the formation of the LiO_2 ground state.

3.2. Structure and Energy of $Li_{2-x}O_2$ Off-Stoichiometry Phases. To investigate whether topotactic Li removal from Li_2O_2 is possible at the early stage of charging, we evaluate the energy of the off-stoichiometry compositions, $Li_{1.75}O_2$, $Li_{1.50}O_2$, and $Li_{1.25}O_2$. For each of the intermediate composition, we considered a reasonable number of candidate structures by taking into account different arrangements of Li atoms and vacancies, which were generated as follows:

(1) Two symmetrically distinct structures for $Li_{1.50}O_2$ are generated by removing one Li atom from P or L in a single unit cell of Li_2O_2 (see Figure 1a).

(2) We looked at all symmetrically distinct arrangements of Li ions and vacancies in the 1 × 1 × 2 and 2 × 1 × 1 supercells of Li_2O_2. These arrangements yield 6, 12, and 30 structures for the $Li_{1.75}O_2$, $Li_{1.50}O_2$, and $Li_{1.25}O_2$ compositions, respectively.

(3) We further investigated "phase-separated structures" in the 1 × 1 × 4 and 4 × 1 × 1 supercells. "Phase-separated structures" are $Li_{2-x}O_2$ ($0 < x < 1$) structures comprising distinct domains of pure Li_2O_2 and LiO_2 compositions. Among the phase-separated structures, we label the structures as layered (Figure 3a) and channel (Figure 3b) structures. In the layered structure, the domain boundaries are parallel to the $a-b$ plane, whereas in the channel structure, the domain boundaries are in the $a-c$ or $b-c$ plane. We calculated eight $Li_{1.75}O_2$, nine $Li_{1.50}O_2$, and eight $Li_{1.25}O_2$ phase-separated structures.

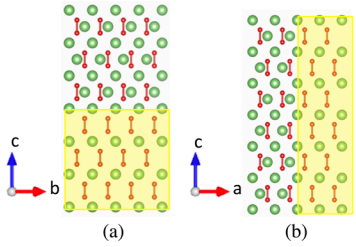

Figure 3. (a) A layered structure of $Li_{2-x}O_2$ ($0 < x < 1$) where Li_2O_2 and LiO_2 phases are separated by the $a-b$ plane, and (b) a channel structure of $Li_{2-x}O_2$ ($0 < x < 1$) where Li_2O_2 and LiO_2 phases are separated by the $a-c$ or $b-c$ planes. Yellow shading is used to highlight LiO_2 regions distinguished from Li_2O_2.

In total, we considered 14, 23, and 38 symmetrically distinct structures for $Li_{1.75}O_2$, $Li_{1.50}O_2$, and $Li_{1.25}O_2$ compositions, respectively. The contribution of the entropy terms to the total energy and the correction energy for O_2 are included as specified in the Computational Methods and the Supporting Information. The values of these corrections and computed formation energies are summarized in Table S4 in the Supporting Information.

Figure 4 shows the energy of a large number of structures between compositions Li_2O_2 and LiO_2 relative to the equilibrium $Li_2O_2-O_2$ tie line. Somewhat surprisingly, there are multiple off-stoichiometric $Li_{2-x}O_2$ configurations that have relatively low energy above the equilibrium state. We find that all of the lowest energy off-stoichiometric structures are layered structures of the type depicted in Figure 3a, in which LiO_2 and Li_2O_2 domains are separated by a boundary in the $a-b$ plane. The lowest energy structures are shown in Figure 5, and their calculated formation enthalpies and lattice parameters are summarized in the Supporting Information. In all of these structures, Li atoms are extracted from the layers that contain the peroxide centers, that is, P sites. Such layer-by-layer Li extraction allows the nearby O_2^- groups to relax without interfering with the peroxide groups in other layers. As more Li are extracted, more such "superoxide" layers are formed. Our results show that the lowest energy structures tend to group

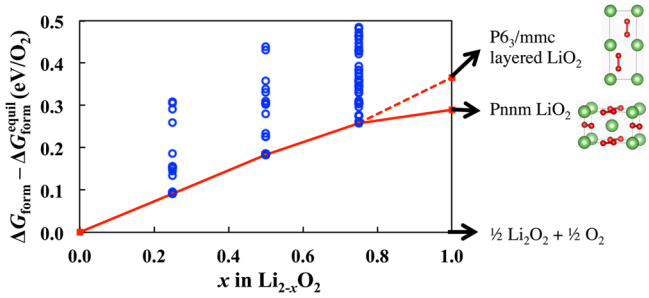

Figure 4. The formation free energy (eV/O_2) of the off-stoichiometry $Li_{2-x}O_2$ structures referenced to the equilibrium in eq 1. The red solid line connects the lowest energy off-stoichiometry $Li_{2-x}O_2$ structures starting from Li_2O_2 with the ground-state structure of LiO_2 ($Pnnm$), whereas the red dashed line ends with the topotactically delithiated $P6_3/mmc$-layered LiO_2 structure.

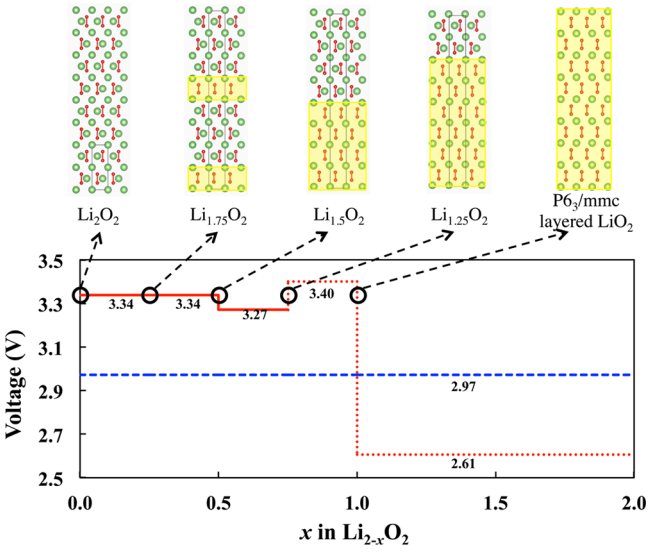

Figure 5. The nonequilibrium voltage profile from Li_2O_2 ($x = 0$) to O_2 ($x = 2$). The red solid and dotted line indicate the predicted topotactic oxidation path. The dashed blue line denotes the direct decomposition of Li_2O_2 into $2Li^+ + 2e^- + O_2$. The lowest energy structures are shown along the path.

dx.doi.org/10.1021/cm401720n | *Chem. Mater.* 2013, 25, 3328−3336

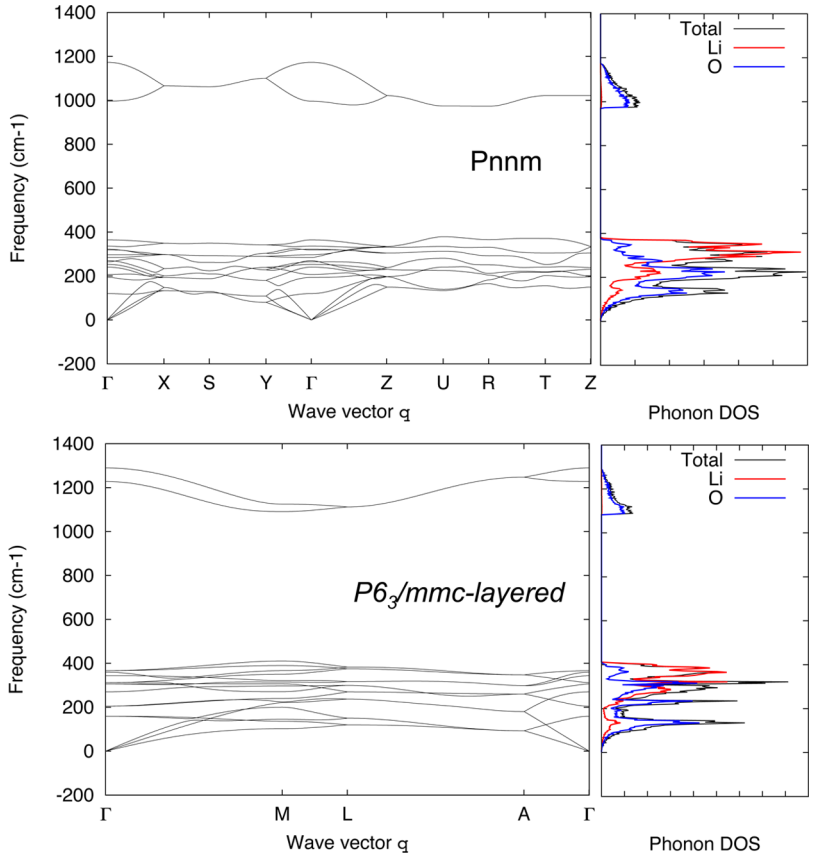

Figure 6. Phonon dispersion and density of states for LiO_2 in the *Pnnm* structure (top) and in the $P6_3/mmc$-layered structure (bottom). The partial phonon densities of states contributed from Li and O are shown in red and blue, respectively.

peroxide and superoxide in layers, probably to minimize strain. Yet the energy of structures where they are grouped but not layered, for example, channel structures, is only marginally higher (see the Supporting Information).

Figure 5 compares the calculated voltage profile for the thermodynamically stable path (blue), and for the metastable path formed from delithiating Li_2O_2 (red). The calculated equilibrium voltage of 2.97 V for the decomposition of Li_2O_2 to $2Li^+ + e^- + O_2$ agrees well with the experimental value of 2.96 V.[48] The red line (solid and dotted) is the metastable voltage profile for topotactic extraction of Li from Li_2O_2. The predicted metastable voltage at 3.34 V is consistent with the experimentally observed charging voltage plateau at 3.1−3.3 V,[2,3,17,25−27] indicating that these off-stoichiometric structures are certainly accessible in the charge process. Because the topotactic delithiation is a nonequilibrium path, its initial charging voltage is above the equilibrium voltage but behaves nonmonotonically as discharge proceeds. This is unlike an equilibrium oxidation profile, which has to have a non-decreasing voltage to satisfy thermodynamic stability conditions. Because the average voltage for two paths between the same compounds is a conserved quantity, the initially higher voltage of the topotactic path has to be compensated by a lower voltage at the end of charge. However, any decrease in voltage along a charging path will lead to instabilities and current localization in the electrode, and hence will not be directly observed, as described later.

3.3. Phonon Spectra for LiO_2 Bulk Structures. To investigate the dynamic stability of LiO_2 structures, we computed the phonon spectra of LiO_2 in its ground state *Pnnm* structure and topotactically delithiated $P6_3/mmc$-layered structure. The phonon calculations for LiO_2 were performed on the basis of the small displacement method within the harmonic approximation using the PHON code.[60] Symmetrically distinct displacements of atoms by 0.04 Å were introduced in a 3 × 3 × 3 supercell for *Pnnm* LiO_2 and a 3 × 3 × 2 supercell for $P6_3/mmc$-layered LiO_2. The lattice parameters and atomic positions of these supercells were optimized in the generalized gradient approximation (GGA) to density functional theory. Unit cells of both structures were relaxed until the total energies and forces were converged to within 10^{-7} eV and 10^{-3} eV/Å per formula unit, and the phonon density of states (DOS) was computed on the basis of 25 × 20 × 30 and 30 × 30 × 18 *q*-points grid for *Pnnm* and $P6_3/mmc$-layered LiO_2, respectively. To keep the computational costs reasonable, the phonon calculations were performed using the GGA instead of the HSE functional.

No imaginary vibrational frequency appears in the computed phonon dispersion in both *Pnnm* and $P6_3/mmc$-layered LiO_2 (Figure 6), which suggests that both LiO_2 structures are dynamically stable. The phonon spectra of *Pnnm* and $P6_3/mmc$-layered LiO_2 show some common features, such as (i) a broad phonon band at low frequencies, which is relatively flat in the wave vector space and has contributions from both cations and anions, (ii) a wide phonon band gap in the range of 380−970 cm^{-1} for *Pnnm*, and of 410−1085 cm^{-1} for $P6_3/mmc$-layered, and (iii) a localized phonon band at high frequencies arising from the O_2^- anions. The O_2^- vibration modes have higher frequencies for $P6_3/mmc$-layered LiO_2 (ranging from 1085 to 1290 cm^{-1}) than for *Pnnm* (ranging from 970 to 1173 cm^{-1}),

dx.doi.org/10.1021/cm401720n | *Chem. Mater.* 2013, 25, 3328−3336

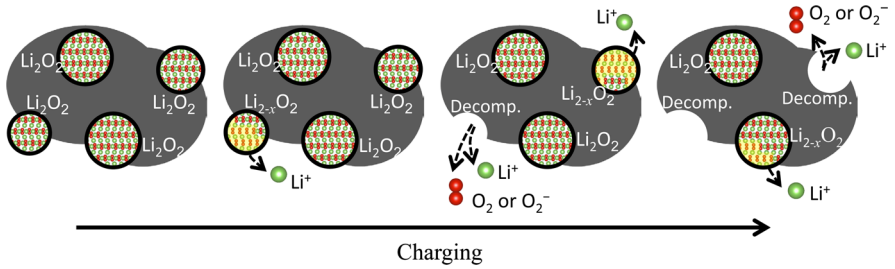

Figure 7. A facile off-stoichiometric mechanism of charging in Li−O_2 batteries. Because of the nonmonotonic voltage profile upon charging (Figure 5), only a few Li_2O_2 particles are involved in the topotactic delithiation at any given time.

indicating that the O_2^- bonds in $P6_3/mmc$-layered LiO_2 are stronger than those in *Pnnm* LiO_2. The peak frequency of the O_2^- vibrational mode in the phonon DOS (Figure 6) is located at 1089 cm^{-1} for $P6_3/mmc$-layered LiO_2, which is comparable to the experimentally detected O−O stretching frequencies of LiO_2 monomer gas (1094 cm^{-1})[61,62] and an isolated O_2^- radical (1090 cm^{-1}).[63] More importantly, the Raman peak for LiO_2 is observed at 1125 cm^{-1} during the operation of Li−O_2 batteries,[30] which agrees with the O_2^- vibrational mode for $P6_3/mmc$-layered LiO_2. The peak frequency for the O_2^- vibrational mode for *Pnnm*, on the other hand, is located at 996 cm^{-1}, which is significantly lower than the value of 1103 cm^{-1} reported in previous computational works by analyzing the Γ−X−S−Y−Γ segment for *Pnnm* LiO_2.[30,59] Our lower frequencies, however, occurred along the Z−U−R−T−Z high symmetry *q*-lines for the O_2^- phonon branch, which was not reported in the previous work.[59] Therefore, the LiO_2 in $P6_3/mmc$-layered structure rather than *Pnnm* structure can be a possible structure that accounts for the peak at 1125 cm^{-1} observed in the Raman spectrum during the operation of Li−O_2 battery.[30]

4. DISCUSSION

One tends to think of polarization in electrochemical experiments as the extra force required to drive the equilibrium reaction forward (e.g., to overcome nucleation barriers, Li^+ or electron transport problems, or catalytic barriers). Yet our results demand a different viewpoint: When the equilibrium voltage is applied, the chemical potential of Li in the system is such that only the equilibrium reaction can proceed. Yet once an overpotential is applied, the number of accessible paths becomes much larger: any path along which the required voltage remains below the applied voltage can be used by the system. Out of all of these possible reaction paths, the one that proceeds the fastest is the one the system will pick. One should therefore think of overpotential as "enabling more reactions paths", rather than making the thermodynamic path faster. Similar arguments have been made to understand conversion reactions[64] and in understanding the rapid kinetics of the first-order phase transition in $LiFePO_4$ upon charging and discharging.[65]

An off-stoichiometric path is likely to be a facile path for transformation: multiple theoretical studies indicate that once vacancies are created, the mobility of Li vacancy in Li_2O_2 is high with a migration energy of ∼0.3−0.4 eV.[37−39] In addition, the energy to create Li vacancies has been predicted to be as low as ∼0.1−0.3 eV on the top layer of the Li_2O_2 surfaces.[31,35] Li^+ removal also creates electronic holes that have reasonably low activation barrier for motion.[36] Good electronic conductivity can therefore be expected in off-stoichiometric peroxide particles.

We first discuss the mechanism by which a single particle of Li_2O_2 can decompose, and then evaluate the consequences for the multiparticle electrode behavior. To charge Li_2O_2, both Li and oxygen have to be removed. It has typically been assumed that Li_2O_2 is stoichiometric and hence both Li and oxygen have to be removed at the same rate from the particle, apart from stoichiometry variations in the surface layer.[35] Our results indicate that simultaneous oxygen and Li removal is not the only option: Off-stoichiometric delithiation with local superoxide ion formation in the material can proceed at low overpotential without leading to mechanical instability in the structure. The off-stoichiometric phase is easy to form during charging, given the low formation energy of bulk $Li_{2-x}O_2$ phases, which is thermodynamically accessible under a small overpotential. More importantly, the attraction among Li vacancies and the energetic preference of Li vacancies to P sites facilitates the clustering of Li vacancies and the nucleation of LiO_2 layers in the Li_2O_2 framework (Figures 3 and 5). Because Li mobility is expected to be good, in the off-stoichiometric material as well as in the electrolyte, and oxygen evolution from the surface on the other hand seems to be hindered by a substantial barrier,[35] it is likely that oxygen removal lags behind Li removal, creating substoichiometric $Li_{2-x}O_2$ states in a particle. What the nature of "*x*" is will depend on the relative O_2 versus Li removal rate, and hence on the particle size, electronic wiring, and electrolyte. In the limit where O_2 removal is very slow, a particle will homogenously delithiate until it reaches a critical value of *x* where it dissolves in the electrolyte. Yet we will argue below that even under this scenario, such metastable off-stoichiometric states will be difficult to observe as they lead to inhomogeneous reactions. Nonetheless, they are critical to understand the kinetics and atomistic-level mechanism of Li_2O_2 charging.

Our findings apply to the reaction path that a single Li_2O_2 peroxide particle takes. How such single particle behavior manifests itself at the macroscopic electrode scale, which consists of a large number of interacting particles, depends on the shape of the voltage profile, and on the electrode construction. An important consequence is that the nonmonotonic topotactic voltage profile in Figure 5 will lead to an inhomogeneous reaction of the electrode (see Figure 7). Apart from the small voltage increase as *x* reaches 0.75 in Figure 5, the voltage is either constant or decreasing as the charge increases, indicating that once delithiation of the peroxide starts, it will proceed rapidly and locally (under constant applied voltage) because the driving force for Li removal increases with increasing state of charge (a condition opposite to a thermodynamic equilibrium path). Once this reaction

dx.doi.org/10.1021/cm401720n | *Chem. Mater.* 2013, 25, 3328−3336

starts in a particle, it will continue at the maximum rate consistent with the Li^+ and hole mobility in the solid. At some level of delithiation, this particle will become unstable and either dissolve in the electrolyte or release O_2. Figure 4 shows that the excess energy (above the equilibrium) of the delithiated peroxide increases with x, indicating that the structures become more and more unstable as x increases in $Li_{2-x}O_2$. The lower plateau at 2.61 V at $x > 1$ in Figure 5 corresponds to the decomposition potential of LiO_2. This potential is well below the typical charging voltage and hence no long-lived LiO_2 is expected in the charge process, which is confirmed by in situ SERS characterization.[21] Interestingly, our predicted potential for LiO_2 is very close to the typical discharge potentials seen in Li−air cells,[2,3] consistent with the fact that the first step in discharge is the formation of the metastable superoxide. However, in charge, either decomposition before $x = 1$ occurs, or topotactic delithiation of Li_2O_2 to LiO_2 occurs, with the LiO_2 immediately decomposing. In either case, the superoxide will not be observed.

When the charging mechanism occurs along the topotactic delithiation pathway to $Li_{2-x}O_2$, near $x = 1$, one possibility is that LiO_2 may simply dissolve into the electrolyte[42] and the last oxidation step of O_2^- to O_2 may occur on the surfaces of the electrode pores or at catalytic additives present.[10,12,23,24,66] If the material disintegrates for $x < 1$, then some amount of disproportionation will occur of $Li_{2-x}O_2$ into $(1-x)Li_2O_2 + xLiO_2$, which with dissolution of the superoxide would lead to $(1-x)Li_2O_2 + x[Li^+] + x[O_2^-]$.[20,22,67]

It is important to stress that our results provide a mechanism by which Li_2O_2 particles can lose Li upon charging, but they do not argue that the electrode as a whole goes homogenously through these off-stoichiometric states. Two factors will promote nonhomogeneous charging. The shape of the predicted voltage profile along the nonequilibrium path drives localization of current in the electrode as it leads to accelerated charging of the particles that, due to their size or connectivity and position in the electrode, proceed first in delithiation. A secondary effect is that the particles that charge first will locally inject Li^+ and oxygen species in the electrolyte at a high rate when they decompose, and drop the local potential, preventing nearby Li_2O_2 particles from reacting until the excess Li^+ and oxygen are removed by diffusion through the electrode porosity. This local particle-by-particle charging illustrated in Figure 7 has been observed in experiments.[12] The scanning electron microscopy (SEM) characterization by Harding et al.[12] has shown that the electrode charged by 50% reveals a reduced number of Li_2O_2 particles, while the size of the remaining Li_2O_2 particles remains the same as before charging. Neither the direct surface decomposition[35,37] nor the stepped surface facilitated mechanism[26,31,37] can explain this inhomogeneous decomposition mechanism at the beginning of charge in Li−O_2 batteries. Our proposed mechanism also agrees with the experimental and computational observation of the existence of LiO_2-like species,[30,68] which account for the initial 40% of charging capacity at a voltage plateau ∼3.2−3.5 V. Yang et al.[30] attributed the observed Raman spectrum peak at ∼1125 cm^{-1} to the LiO_2-like species on the surface of small $(Li_2O_2)_n$ clusters (n = 3−4, 16). However, it is unlikely for surfaces or small clusters to account for ∼30−50% of charging capacity, given that Li_2O_2 particles sizes are as large as tens to hundreds of nanometers. On the other hand, the topotactic delithiation may contribute to a significant amount of charging capacity, and the topotactically delithiated $P6_3/mmc$-layered LiO_2 phase yields O_2^- vibrational frequency that is consistent with the experimental Raman spectra. This vibrational peak of superoxides in the Raman spectra has been attributed to the initial charging capacity at the low charging voltage plateau.

The localization of the instantaneous reaction may make it difficult to observe the off-stoichiometric states during charge as they immediately proceed to charge completely under constant applied voltage according to Figure 5. Nonetheless, as these constitute the path by which particles charge, they are important to understand the overpotential and kinetics of Li−air.

This inhomogeneous reaction is also important to understand why O_2 evolution starts at the same time as the onset of the charging current as documented in refs 2 and 17. We predict that at any given time, only a small fraction of the particles are participating in the charging process. Some of these particles may be in the initial delithiation process, while others, which reached the delithiation step earlier due to their size or position in the electrode, are in the process of fully decomposing and releasing O_2. Hence, while for a single particle the Li^+ extraction and O_2 evolution do not coincide according to eq 1, on average at the electrode level they will evolve in a ratio of two to one, as is seen in experiments.[2,17]

Our proposed reaction path successfully reveals the origin of the low charging voltage plateau at 3.2−3.3 V at the initial stage of charging. This reaction path is also consistent with the relatively higher rate and other observed phenomena in the corresponding experiments. Our proposed reaction path only accounts for part of the charging process at the low overpotential. Further studies are required to understand whether the increase in charging voltage after the initial 30−50% charge is due to intrinsic features of Li_2O_2 decomposition, or due to electrode design issues. In that context, it is important to understand that, according to our proposed mechanism, the smaller and better connected particles (electronically and ionically) will fully charge first, leaving the larger and poorly connected particles uncharged until the later part of the charge is reached as depicted in Figure 7. Hence, a strong degradation of the kinetics toward the later part of charge is expected from our mechanistic model.

The consequences of our findings are significant. At the single particle level, we predict a facile path to recharge a Li−air battery once some overpotential is applied. If this is the only path with reasonable reaction kinetics, then this overpotential sets a minimum bound on the charge potential of a Li−air system. However, given the low formation energy of $Li_{2-x}O_2$ phases and good ionic conductivity in $Li_{2-x}O_2$, one can reasonably infer that at this overpotential the local rate of Li removal from a Li_2O_2 particle is fast, pointing at the exciting possibility to create fast charging Li−air systems, once the transport issues at the electrode level and electrolyte, rather than at the particle level, are resolved. We believe that resolving the current density limitations in Li−air is one of the significant obstacles toward technological application, and that our findings indicate that there are no obstacles to this at the Li_2O_2 particle level.

5. CONCLUSIONS

In this study, we presented an ab initio computation study on the charging reaction path of Li_2O_2. We identify the *Pnnm* structure as the ground-state structure for LiO_2 and the $P6_3/mmc$ layered structure as the topotactically delithiated Li_2O_2 structures, which has a reasonably low formation energy. Our

dx.doi.org/10.1021/cm401720n | *Chem. Mater.* 2013, 25, 3328−3336

calculations reveal that the reaction, $Li_2O_2 \rightarrow 2Li^+ + 2e^- + O_2$, is indeed the equilibrium path of oxidation of Li_2O_2. We propose and demonstrate topotactic delithiation of Li_2O_2 to form off-stoichiometric $Li_{2-x}O_2$ compounds as a facile oxidization path, which is similar to the charging mechanism in typical Li-ion intercalation electrodes. An overpotential as low as ~0.3−0.4 V is required for this topotactic delithiation pathway, which is kinetically preferred to the thermodynamic equilibrium path. In addition, the topotactic delithiation mechanism suggests localized oxidization of the particles, which leads to particle-by-particle inhomogeneous decomposition during charging. In summary, our results support recent experimental findings on fast kinetics and low overpotential in $Li-O_2$ batteries and, more importantly, suggest a possibility of fast charging $Li-O_2$ batteries.

■ ASSOCIATED CONTENT

Supporting Information

Lattice parameters for *Pnnm* and $P6_3/mmc$-layered LiO_2 and Li_2O_2; the correction energy for oxides, peroxides, and superoxides; energetics of $Li_{2-x}O_2$ (x = 0.25, 0.50, and 0.75) structures referencing the equilibrium path; and a summary of energy and entropy values used (PDF). This material is available free of charge via the Internet at http://pubs.acs.org.

■ AUTHOR INFORMATION

Corresponding Author

*E-mail: gceder@mit.edu.

Notes

The authors declare no competing financial interest.

■ ACKNOWLEDGMENTS

We gratefully acknowledge multiple insightful discussions with Professor Shao-Horn and her research group. This work was supported by the MRSEC Program of the National Science Foundation under contract DMR − 0819762, and by the CERC-CVC US China Clean Energy Research Center-Clean Vehicle Consortium of the Department of Energy under award number DE − PI0000012. Computing resources were provided through TeraGrid by the Texas Advanced Computing Center (TACC) under grant number TG-DMR970008S.

■ REFERENCES

(1) Abraham, K. M.; Jiang, Z. *J. Electrochem. Soc.* **1996**, *143*, 1.
(2) Peng, Z. Q.; Freunberger, S. A.; Chen, Y. H.; Bruce, P. G. *Science* **2012**, *337*, 563.
(3) Jung, H.-G.; Hassoun, J.; Park, J.-B.; Sun, Y.-K.; Scrosati, B. *Nat. Chem.* **2012**, *4*, 579.
(4) Ogasawara, T.; Debart, A.; Holzapfel, M.; Novak, P.; Bruce, P. G. *J. Am. Chem. Soc.* **2006**, *128*, 1390.
(5) Black, R.; Adams, B.; Nazar, L. F. *Adv. Energy Mater.* **2012**, *2*, 801.
(6) Christensen, J.; Albertus, P.; Sanchez-Carrera, R. S.; Lohmann, T.; Kozinsky, B.; Liedtke, R.; Ahmed, J.; Kojic, A. *J. Electrochem. Soc.* **2012**, *159*, R1.
(7) Bruce, P. G.; Freunberger, S. A.; Hardwick, L. J.; Tarascon, J.-M. *Nat. Mater.* **2012**, *11*, 19.
(8) Lee, J. S.; Kim, S. T.; Cao, R.; Choi, N. S.; Liu, M.; Lee, K. T.; Cho, J. *Adv. Energy Mater.* **2011**, *1*, 34.
(9) Girishkumar, G.; McCloskey, B.; Luntz, A. C.; Swanson, S.; Wilcke, W. *J. Phys. Chem. Lett.* **2010**, *1*, 2193.
(10) Shao, Y. Y.; Park, S.; Xiao, J.; Zhang, J. G.; Wang, Y.; Liu, J. *ACS Catal.* **2012**, *2*, 844.
(11) Lu, Y. C.; Kwabi, D. G.; Yao, K. P. C.; Harding, J. R.; Zhou, J. G.; Zuin, L.; Shao-Horn, Y. *Energy Environ. Sci.* **2011**, *4*, 2999.
(12) Harding, J. R.; Lu, Y. C.; Tsukada, Y.; Shao-Horn, Y. *Phys. Chem. Chem. Phys.* **2012**, *14*, 10540.
(13) Xu, W.; Viswanathan, V. V.; Wang, D. Y.; Towne, S. A.; Xiao, J.; Nie, Z. M.; Hu, D. H.; Zhang, J. G. *J. Power Sources* **2011**, *196*, 3894.
(14) Black, R.; Oh, S. H.; Lee, J. H.; Yim, T.; Adams, B.; Nazar, L. F. *J. Am. Chem. Soc.* **2012**, *134*, 2902.
(15) Mizuno, F.; Nakanishi, S.; Kotani, Y.; Yokoishi, S.; Iba, H. *Electrochemistry* **2010**, *78*, 403.
(16) Freunberger, S. A.; Chen, Y. H.; Drewett, N. E.; Hardwick, L. J.; Barde, F.; Bruce, P. G. *Angew. Chem., Int. Ed.* **2011**, *50*, 8609.
(17) McCloskey, B. D.; Bethune, D. S.; Shelby, R. M.; Girishkumar, G.; Luntz, A. C. *J. Phys. Chem. Lett.* **2011**, *2*, 1161.
(18) Freunberger, S. A.; Chen, Y. H.; Peng, Z. Q.; Griffin, J. M.; Hardwick, L. J.; Barde, F.; Novak, P.; Bruce, P. G. *J. Am. Chem. Soc.* **2011**, *133*, 8040.
(19) Xiao, J.; Hu, J. Z.; Wang, D. Y.; Hu, D. H.; Xu, W.; Graff, G. L.; Nie, Z. M.; Liu, J.; Zhang, J. G. *J. Power Sources* **2011**, *196*, 5674.
(20) Laoire, C. O.; Mukerjee, S.; Abraham, K. M.; Plichta, E. J.; Hendrickson, M. A. *J. Phys. Chem. C* **2009**, *113*, 20127.
(21) Peng, Z. Q.; Freunberger, S. A.; Hardwick, L. J.; Chen, Y. H.; Giordani, V.; Barde, F.; Novak, P.; Graham, D.; Tarascon, J. M.; Bruce, P. G. *Angew. Chem., Int. Ed.* **2011**, *50*, 6351.
(22) Laoire, C. O.; Mukerjee, S.; Abraham, K. M.; Plichta, E. J.; Hendrickson, M. A. *J. Phys. Chem. C* **2010**, *114*, 9178.
(23) Lu, Y. C.; Gasteiger, H. A.; Shao-Horn, Y. *J. Am. Chem. Soc.* **2011**, *133*, 19048.
(24) Lu, Y. C.; Xu, Z. C.; Gasteiger, H. A.; Chen, S.; Hamad-Schifferli, K.; Shao-Horn, Y. *J. Am. Chem. Soc.* **2010**, *132*, 12170.
(25) McCloskey, B. D.; Scheffler, R.; Speidel, A.; Bethune, D. S.; Shelby, R. M.; Luntz, A. C. *J. Am. Chem. Soc.* **2011**, *133*, 18038.
(26) McCloskey, B. D.; Speidel, A.; Scheffler, R.; Miller, D. C.; Viswanathan, V.; Hummelshoj, J. S.; Norskov, J. K.; Luntz, A. C. *J. Phys. Chem. Lett.* **2012**, *3*, 997.
(27) Zhang, Z.; Lu, J.; Assary, R. S.; Du, P.; Wang, H.-H.; Sun, Y.-K.; Qin, Y.; Lau, K. C.; Greeley, J.; Redfern, P. C.; Iddir, H.; Curtiss, L. A.; Amine, K. *J. Phys. Chem. C* **2011**, *115*, 25535.
(28) Lu, Y.-C.; Crumlin, E. J.; Veith, G. M.; Harding, J. R.; Mutoro, E.; Baggetto, L.; Dudney, N. J.; Liu, Z.; Shao-Horn, Y. *Sci. Rep.* **2012**, *2*.
(29) Jung, H.-G.; Kim, H.-S.; Park, J.-B.; Oh, I.-H.; Hassoun, J.; Yoon, C. S.; Scrosati, B.; Sun, Y.-K. *Nano Lett.* **2012**, *12*, 4333.
(30) Yang, J.; Zhai, D.; Wang, H.-H.; Lau, K. C.; Schlueter, J. A.; Du, P.; Myers, D. J.; Sun, Y.-K.; Curtiss, L. A.; Amine, K. *Phys. Chem. Chem. Phys.* **2013**, *15*, 3764.
(31) Hummelshøj, J. S.; Luntz, A. C.; Nørskov, J. K. *J. Chem. Phys.* **2013**, *138*, 034703.
(32) McCloskey, B. D.; Scheffler, R.; Speidel, A.; Girishkumar, G.; Luntz, A. C. *J. Phys. Chem. C* **2012**, *116*, 23897.
(33) Oh, S. H.; Nazar, L. F. *Adv. Energy Mater.* **2012**, *2*, 903.
(34) Lu, Y.-C.; Shao-Horn, Y. *J. Phys. Chem. Lett.* **2012**, *4*, 93.
(35) Mo, Y. F.; Ong, S. P.; Ceder, G. *Phys. Rev. B* **2011**, *84*, 1.
(36) Ong, S. P.; Mo, Y. F.; Ceder, G. *Phys. Rev. B* **2012**, *85*, 2.
(37) Hummelshøj, J. S.; Blomqvist, J.; Datta, S.; Vegge, T.; Rossmeisl, J.; Thygesen, K. S.; Luntz, A. C.; Jacobsen, K. W.; Nørskov, J. K. *J. Chem. Phys.* **2010**, *132*, 071101.
(38) Chen, J.; Hummelshoj, J. S.; Thygesen, K. S.; Myrdal, J. S. G.; Norskov, J. K.; Vegge, T. *Catal. Today* **2011**, *165*, 2.
(39) Radin, M. D.; Rodriguez, J. F.; Tian, F.; Siegel, D. J. *J. Am. Chem. Soc.* **2012**, *134*, 1093.
(40) Zhao, Y. F.; Ban, C. M.; Kang, J.; Santhanagopalan, S.; Kim, G. H.; Wei, S. H.; Dillon, A. C. *Appl. Phys. Lett.* **2012**, *101*.
(41) Viswanathan, V.; Thygesen, K. S.; Hummelshoj, J. S.; Norskov, J. K.; Girishkumar, G.; McCloskey, B. D.; Luntz, A. C. *J. Chem. Phys.* **2011**, *135*, 214704.
(42) Bryantsev, V. *Theor. Chem. Acc.* **2012**, *131*, 1.
(43) Kresse, G.; Furthmuller, J. *Phys. Rev. B* **1996**, *54*, 11169.
(44) Blochl, P. E. *Phys. Rev. B* **1994**, *50*, 17953.
(45) Heyd, J.; Scuseria, G. E.; Ernzerhof, M. *J. Chem. Phys.* **2003**, *118*, 8207.

(46) Heyd, J.; Scuseria, G. E.; Ernzerhof, M. *J. Chem. Phys.* **2006**, *124*, 219906.
(47) Paier, J.; Marsman, M.; Hummer, K.; Kresse, G.; Gerber, I. C.; Angyan, J. G. *J. Chem. Phys.* **2006**, *125*, 249901.
(48) Chase, M. W. *National Institute of Science and Technology NIST-JANAF Thermochemical Tables*; American Chemical Society; American Institute of Physics for the National Institute of Standards and Technology: [Washington, DC]; Woodbury, NY, 1998.
(49) Aydinol, M. K.; Kohan, A. F.; Ceder, G.; Cho, K.; Joannopoulos, J. *Phys. Rev. B* **1997**, *56*, 1354.
(50) Chevrier, V. L.; Ong, S. P.; Armiento, R.; Chan, M. K. Y.; Ceder, G. *Phys. Rev. B* **2010**, *82*, 075122.
(51) Wang, L.; Maxisch, T.; Ceder, G. *Phys. Rev. B* **2006**, *73*, 1.
(52) Cota, L. G.; de la Mora, P. *Acta Crystallogr., Sect. B* **2005**, *61*, 133.
(53) Chan, M. K. Y.; Shirley, E. L.; Karan, N. K.; Balasubramanian, M.; Ren, Y.; Greeley, J. P.; Fister, T. T. *J. Phys. Chem. Lett.* **2011**, *2*, 2483.
(54) Radin, M. D.; Rodriguez, J. F.; Siegel, D. J. *Lithium Peroxide Surfaces and Point Defects: Relevance for Li−Air Batteries*; Battery Congress: Ann Arbor, MI, 2011.
(55) Yanli, W.; Yi, D.; Jun, N. *J. Phys.: Condens. Matter* **2009**, *21*, 035401.
(56) Xiao, R.; Li, H.; Chen, L. *Chem. Mater.* **2012**, *24*, 4242.
(57) Bakulina, V. M.; Tokareva, S. A.; Vol'nov, I. I. *J. Struct. Chem.* **1967**, *8*, 980.
(58) Seriani, N. *Nanotechnology* **2009**, *20*, 445703.
(59) Lau, K. C.; Curtiss, L. A.; Greeley, J. *J. Phys. Chem. C* **2011**, *115*, 23625.
(60) Alfe, D. *Comput. Phys. Commun.* **2009**, *180*, 2622.
(61) Wang, X.; Andrews, L. *Mol. Phys.* **2009**, *107*, 739.
(62) Andrews, L. *J. Chem. Phys.* **1969**, *50*, 4288.
(63) Rolfe, J.; Holzer, W.; Murphy, W. F.; Bernstein, H. J. *J. Chem. Phys.* **1968**, *49*, 963.
(64) Doe, R. E.; Persson, K. A.; Meng, Y. S.; Ceder, G. *Chem. Mater.* **2008**, *20*, 5274.
(65) Malik, R.; Zhou, F.; Ceder, G. *Nat. Mater.* **2011**, *10*, 587.
(66) Debart, A.; Paterson, A. J.; Bao, J.; Bruce, P. G. *Angew. Chem., Int. Ed.* **2008**, *47*, 4521.
(67) Lim, H.-K.; Lim, H.-D.; Park, K.-Y.; Seo, D.-H.; Gwon, H.; Hong, J.; Goddard, W. A.; Kim, H.; Kang, K. *J. Am. Chem. Soc.* **2013**, *135*, 9733.
(68) Lau, K. C.; Assary, R. S.; Redfern, P.; Greeley, J.; Curtiss, L. A. *J. Phys. Chem. C* **2012**, *116*, 23890.